Fetal Zika virus inoculation in macaques revealed control of the fetal viral load during pregnancy

Charles Egloff, Claire-Maëlle Fovet, Jessica Denis, Quentin Pascal, Laetitia Bossevot, Sophie Luccantoni, Marco Leonec, Nathalie Dereuddre-Bosquet, Isabelle Leparc-Goffart, Roger Le Grand, et al.

Virology Journal

RESEARCH

Open Access

Fetal Zika virus inoculation in macaques revealed control of the fetal viral load during pregnancy

Charles Egloff[1,2], Claire-Maëlle Fovet[1], Jessica Denis[3], Quentin Pascal[1], Laetitia Bossevot[1], Sophie Luccantoni[1], Marco Leonec[1], Nathalie Dereuddre-Bosquet[1], Isabelle Leparc-Goffart[4,5], Roger Le Grand[1], Guillaume André Durand[4,5], Cyril Badaut[4,6], Olivier Picone[2] and Pierre Roques[1,7*]

Abstract

Background Early pregnancy Zika virus (ZIKV) infection is associated with major brain damage in fetuses, leading to microcephaly in 0.6–5.0% of cases, but the underlying mechanisms remain largely unknown.

Methods To understand the kinetics of ZIKV infection during fetal development in a nonhuman primate model, four cynomolgus macaque fetuses were exposed in utero through echo-guided intramuscular inoculation with 10^3 PFU of ZIKV at 70–80 days of gestation, 2 controls were mock inoculated. Clinical, immuno-virological and ultrasound imaging follow-ups of the mother/fetus pairs were performed until autopsy after cesarean section 1 or 2 months after exposure (n = 3 per group).

Results ZIKV was transmitted from the fetus to the mother and then replicate in the peripheral blood of the mother from week 1 to 4 postexposure. Infected fetal brains tended to be smaller than those of controls, but not the femur lengths. High level of viral RNA ws found after the first month in brain tissues and placenta. Thereafter, there was partial control of the virus in the fetus, resulting in a decreased number of infected tissue sections and a decreased viral load. Immune cellular and humoral responses were effectively induced.

Conclusions ZIKV infection during the second trimester of gestation induces short-term brain injury, and although viral genomes persist in tissues, most of the virus is cleared before delivery.

Keywords TORCH infection, Viral clearance, Microcephaly, Neutralizing antibodies, Nonhuman primate model, Zika virus

*Correspondence:
Pierre Roques
pierre.roques@cea.fr; pierre.roques@pasteur.fr
[1] Center for Immunology of Viral, Auto-Immune, Hematological and Viral Diseases (IMVA-HB/IDMIT), Université Paris-Saclay, Inserm, CEA, 92265 Fontenay aux Roses, France
[2] Service de gynécologie-obstétrique, Hôpital Louis Mourier, AP-HP, IAME INSERM U1137, Université de PARIS, Paris, France
[3] Unité interactions hôtes-pathogènes, Institut de Recherche Biomédicale des Armées, 91223 Brétigny-sur-Orge, France
[4] Unité des Virus Émergents (UVE: Aix-Marseille Univ-Corsica Univ-IRD 190-Inserm 1207-IRBA), 13005 Marseille, France
[5] National Reference Center for Arboviruses, INSERM-Institut de Recherche Biomédicale des Armées, 13005 Marseille, France
[6] Unité de Virologie, Institut de Recherche Biomédicale des Armées, 91223 Brétigny-sur-Orge, France
[7] Present Address: Virology Unit, Institut Pasteur de Guinée (IPGui), BP4416, Conakry, Guinea

Introduction

Zika virus (ZIKV) is a flavivirus that is transmitted mainly by *Aedes albopictus* and *Aedes aegypti* mosquitoes; ZIKV was discovered in 1947 in the Zika forest of Uganda during surveillance of rhesus monkeys via sentinel platforms [1]. Major epidemics in 2015 in South and Central America revealed fetal brain developmental defects associated with ZIKV maternal infection during pregnancy. Since then, research has focused on understanding the mechanisms of pathogenesis, but limited access to human samples has advocated for the need for relevant animal models.

Nonhuman primates (NHPs) are a model of choice for in vivo infection studies during pregnancy because they share similarities with humans in terms of gestational and neurodevelopmental timelines, immune system, uterine anatomy, singleton gestation, hemochorial placentation, endocrine control of parturition and vaginal microbiome [2]. In addition, the brains of both humans and NHPs require a long maturation process that ends after birth [3, 4].

To date, in rodent animal models, a gestational stage effect has been observed in many studies, with worse fetal outcomes following ZIKV infection at earlier gestational stages [5]. One of the major disadvantages of rodent models, in addition to placentation type differences, is that the duration of pregnancy is relatively short compared to that in humans. Therefore, the mechanisms associated with the timing of both the exposure and brain maturation are mainly representative of the most severe cases but not of the majority of mildly affected human infants. Furthermore, the lack of susceptibility of wild-type mice to various strains of ZIKV necessitates the use of immune-defective mice to further complicate disease modeling [6].

Maternal infection during pregnancy is characterized by prolonged maternal viremia and may cause damage to the fetal brain and placenta. Studies of ZIKV during pregnancy have reported increased rates of congenital Zika syndrome when infection occurs early in pregnancy [7]. Many viral infections in pregnant women might be associated with miscarriage [8] Thus, ZIKV infections during pregnancy are also accountable, in certain circumstances, for abortive events [9, 10]. Cerebral ZIKV infection in fetuses is responsible for neuro-progenitor damage, with cell apoptosis responsible for destruction of the cerebral parenchyma and disorganization of the architecture [11]. After maternal ZIKV infection in the NHP model, studies revealed uncertain maternal–fetal transmission with a variable viral load in fetal brain tissue. Fetal abnormalities and brain injury were variable and usually moderate [12]. Cerebral tissues from these fetuses euthanized at term revealed inflammation, a decrease in neuronal progenitors, calcification, vascularization, and modifications of the cellular mechanisms of stem cells [6, 13, 14].

Most studies in the NHP have focused on fetal status close to delivery at the end of fetal maturation or on infant neuropathological outcomes, while the evolution of viral pathogenesis and immune responses during pregnancy from infection to term are still unknown [13, 15–24].

Nonetheless, there is still a clear need to develop additional NHP models to study the evolution of pathogenesis after ZIKV infection during pregnancy. A better understanding of the evolution of the pathological process during pregnancy is essential for determining the appropriate fetal treatment. Indeed, for in utero treatment to be effective, it is necessary to know whether the development of lesions is progressive. Herein, in this new NHP model involving pregnant *Macaca fascicularis* dams and fetuses, to precisely control the timing of the infection, we inoculated ZIKV directly into fetuses in utero via an ultrasound-guided intramuscular route. We describe the exposure of four cynomolgus macaque fetuses to a French Polynesian ZIKV strain and its viral evolution during pregnancy in dams and fetuses, with a focus on fetal infection at either 30 days or 60 days postexposure, thus revealing the early and late stages of in utero ZIKV infection, respectively.

Methods

Animals

Six pregnant female cynomolgus macaques (*Macaca fascicularis*), 5–10 years old and weighing > 3 kg, were imported from Mauritius (negative for Zika virus and Dengue virus). NHP were housed in IDMIT infrastructure BSL3 facilities (CEA, Fontenay-aux-Roses, France) in accordance with French national regulations (Authorization number #D92-032-02 for animal use). The CEA was established in accordance with the ETS123 recommendations of the European Directive 2010/63/CE and the Standards for Human Care and Use of Laboratory Animals (OLAW number #A5826-01). The studies were approved by the institutional ethical committee (CEtEA #44) and authorized by the French Research, Innovation and Education Ministry under registration number APAFIS#6805-20160920 171672 v4.

For all procedures, animals were sedated with 10 mg/kg ketamine chlorhydrate via the intramuscular route (Imalgen 1000®, Rhône-Mérieux, Lyon, France) or with 5 mg/kg xylazine via the intramuscular route (Rompun®, Bayer/Elanco Animal Health, Neuilly sur-Seine, France) for virus inoculation, imaging and blood collection or with ketamine chlorhydrate and diazepam 0.25 mg/kg via the intramuscular route (Valium®, Roche, Boulogne-Billancourt, France) for caesarian sectioning. For surgical

interventions, animals received an appropriate analgesic treatment and were monitored by veterinary and animal care staff for adverse reactions and signs of disease. Euthanasia was performed after anesthesia using 180 mg/kg pentobarbital (Doléthal®, Vetoquinol SA, Lure, France).

Viral stock and in utero *inoculations*

The ZIKV strain H/PF/13 was collected from human serum in French Polynesia in 2013 [25] and obtained from the EVAg program (https://www.european-virus-archive.com). The strain was amplified from C6/36 mosquito cells and titrated with VERO E6 cells to a concentration of 2×10^8 TCID50/mL.

The dams were sedated, and the fetuses were inoculated intramuscularly in the thigh at the most accessible muscle (not specifically identified) with 0.1 mL (1×10^3 pfu) of ZIKV. Control animals were inoculated with saline using the same procedure. Inoculation was performed in utero via a maternal transabdominal route, avoiding placental disks through trans-amniotic membrane ultrasound-guided puncture under aseptic conditions with a 20G/3.5-inch spinal needle at the beginning of the procedure (Fig. 1). The same day, the dams were subjected to amniotic puncture under aseptic conditions before inoculation.

Clinical follow-up

The longitudinal follow-up and sampling methods are summarized in Fig. 1. Animals were observed 7 days a week, and if present, abnormal behavior was reported in a specific single-animal file. During each anesthesia, clinical examination was performed, and body weight and rectal temperature were recorded. Dams were followed for 3 weeks after cesarean section. Blood cell counts, hemoglobin levels and hematocrit levels were determined from blood samples collected with EDTA-coated tubes using an HMX A/L analyzer (Beckman Coulter).

Ultrasound examination

All pregnant females were evaluated weekly using a "General Electric Logiq e" device with a 4.2–13 MHertz probe to perform cerebral morphology and biometric measurements: biparietal diameter (BPD), head circumference (HC), abdominal circumference (AC) and femur length (FL). Reference ranges were plotted using data from Tarantal et al. [26].

Amniocentesis, cesarean section and cord blood sampling

Cesarean section analysis was performed at 32, 34, and 36 days post inoculation for group 1 (BU661, BZ514 and CA953D, respectively) and at 82, 70, and 68 days post inoculation for group 2 (BQ967, BB807C, and

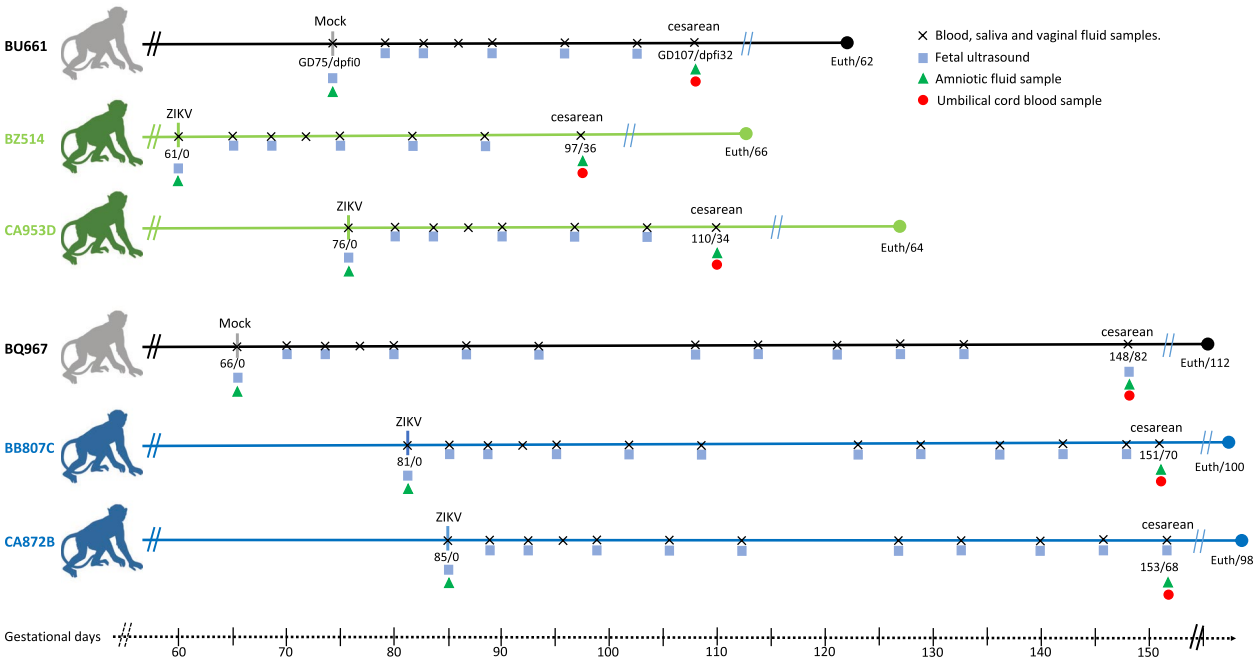

Fig. 1 Study plan. Fetuses were infected intramuscularly with 10^3 pfu ZIKVH/PF/13 on GD 61–85. Serial maternal blood draws and ultrasounds were performed. Fetuses were euthanized for tissue collection following fetal delivery by cesarean section. Infected dams were euthanized 1 month after cesarean section. The animal symbols used are in green for group 1 (cesarean section and fetal euthanasia 1 month after exposure) and blue for group 2 (cesarean section and fetal euthanasia 2 months after exposure); the mock animals are colored in gray for both groups. The data are given as GD/dpfi: gestation day/day post fetal inoculation; Euth/dpfi: female euthanasia/day post fetal inoculation

CA872B, respectively). Before delivery, a 20-gauge 3.5-inch spinal needle was inserted into the ventral abdomen to the amniotic sac by avoiding the placenta with ultrasound guidance to collect 5 mL of amniotic fluid. The fetuses were then exposed, the umbilical cord was sectioned after fetal blood sampling (2 mL), and the two placental discs were removed.

Necropsy

A trained pathologist performed the necropsy and macroscopic analysis of the internal organs, brain and placenta immediately following delivery and euthanasia. Infected dams were euthanized 1 month after surgery. The fetal brains were removed from one block. Left cerebral hemispheres were fixed in 4% paraformaldehyde (PFA; Sigma Aldrich Chimie, St Quentin Falavier, France) for 72 h for histological analysis. The right cerebral hemispheres were dissected according to anatomical zones and immediately frozen for molecular analysis. Biopsies were made for placenta and thoracoabdominal organs, snap-frozen for molecular analysis or fixed in PFA for histological analysis.

Viral quantification in fluids and tissues

In fluids

The plasma viral load was quantified via quantitative RT–PCR using primers amplifying the envelope protein (E) region derived from Lanciotti et al. [27].

Viral RNA was prepared from 100 µL of EDTA-treated anticoagulated, cell-free plasma using the Nucleospin 96 Virus Kit (Macherey Nagel, Düren, Germany; ref: 740452.4). RNA was eluted in 100 µL of nuclease-free water and stored at − 80 °C until analysis. The ZIKV stock was diluted in an EDTA-plasma sample from ZIKV-noninfected macaques, after which a standard curve was generated by serial tenfold dilutions. Standards, controls (+ and −) and viral RNA samples were extracted and tested in parallel as follows. Extracted RNA (10 µL) was reverse transcribed, and PCR was performed using the Superscript One-Step RT–qPCR Kit (ref: 11732088, Invitrogen, Villebon-sur-Yvette, France) in a total 25 µL reaction volume using a CFX96 Touch real-time PCR detection system (Bio-Rad) with the following cycling conditions: 30 min at 56 °C, 5 min at 95 °C, 45 cycles at 95 °C for 15 s and 60 °C for 30 s. All amplifications were performed in duplicate. Standard RNA template dilution had a correlation coefficient of 98–99% over 7 orders of magnitude, with a limit of quantification of 5×10^2 copies of RNA/mL and a limit of detection of 10^2 copies of RNA/mL (Ct < 40).

In tissues

The results of ZIKV RNA RT–qPCR quantification cycle (Cq) were compared to those of cellular GAPDH RNA via a method derived from Labadie et al. 2010 for CHIKV [28].

Tissue lysates were obtained using a Precellys system (Bertin Technologies, Montigny-le-Bretonneux, France) as previously described [29]. Total RNA was extracted in duplicate from lysate aliquots using the Nucleospin 96 RNA Core Kit (Macherey Nagel réf: 740466.4) following the manufacturer's instructions. Relative RT–qPCR was carried out simultaneously with ZIKV primers, a FAM-labeled probe (same as for fluid/plasma samples) and GAPDH primers with a Cyt-5-labeled probe, as described above. RT–qPCR assay efficiencies were determined using standard dilution curves (tenfold serial dilution) for the ZIKV and GAPDH series from a tissue matrix spiked with a known amount of ZIKV viral RNA (Fig. S1). As both amplification reactions were set up to the same efficiency, each ZIKV genomic quantification value was normalized against the GAPDH value in the same sample, and the relative copy number for each sample was calculated with the following equation: Relative copy number $= 2^{-(\text{Cq ZIKV} - \text{Cq GAPDH})}$. The lower limit of detection depends on the amount of GAPDH RNA within the sample and on the quantity of ZIKV RNA (expected to reach 35–38 RT–qPCR Ct), which varies from one tissue to another.

Total RNA was quantified per tissue sample using UV spectroscopy (absorbance at 260 and 280 nm). For each sample and assay, 500 ng of RNA was used; thus, the quantity of ZIKV RNA/ng total RNA was determined. The samples from the standard curve were also normalized to 500 ng of total RNA (50 ng/µL, 10 µL per assay) from tissues per PCR; thus, the final number of ZIKV copies in the standard ranged from 5264×10^3 to 2.1×10^3 copies/ng total RNA. This latter value was fixed as the threshold of our method.

Immune response

Cytokines

Cytokines (G-CSF, GM-CSF, IFN-γ, IL-1β, IL-1rA, IL-2, IL-4, IL-5, IL-6, IL-8, IL-10, IL-12/23 (p40), IL-13, IL-15, MCP-1, MIP-1α, MIP-1β, TGF-α, TNF-α and VEGF) were quantified in EDTA plasma using a 23-plex Milliplex Map Nonhuman Primate Cytokine Magnetic Bead Panel (Merck Millipore, Darmstadt, Germany) and a Bioplex 200 system (Bio-Rad Lab., Marnes-la-Coquette, France) according to the manufacturer's instructions with the addition of an in-house macaque cytokine control [30]. This control was generated by pooling supernatants

of *Macaca fascicularis* PBMCs stimulated with PMA-ionomycine, concanavalin A or LPS.

ELISA responses of sera to inactivated ZIKV

IgG was detected with an inactivated ZIKV-based ELISA as previously described [31]. Briefly, 96-well plates (Maxisorp, NUNC-ImmunoPlate, Thermo Fischer Scientific, Villebon sur Yvette, France) were coated with inactivated ZIKV (the year 1989 African ZIKV strain ArB41644 [32]) diluted (1:200) in PBS. Anti-ZIKV IgG levels were tested with 100 µL of diluted monkey serum samples (1:500). After the washing steps, the IgG was detected with the secondary antibody horseradish peroxidase-conjugated anti-monkey IgG (1/10 000) (Thermo Fisher Scientific). The optical density (OD) was read at 450 nm, and the final value, the OD ratio (ODr), was obtained by dividing the average OD of duplicate wells from the corresponding blank wells coated with uninfected cell culture supernatant treated under the same conditions of ZIKV production and used as a negative control. The threshold of positivity was fixed to an ODr of 3.

Sera neutralization of ZIKV (50% cutoff for the microneutralization assay)

A volume of 120 µL of diluted sera was added to 120 µL of a virus suspension containing 50 TCID50 of the African ZIKV ArB41644 strain from the Central African Republic isolated in 1984 (National Reference Center for Arboviruses collection). The mixture was incubated for 1 h at 37 °C with 5% CO2, after which the mixture was added to Vero cells (ATCC CCL-81, 1.3×10^5 cells/well). After 3.5 days of incubation, the cytopathogenic effects were examined via light microscopy by an experienced operator. The serum neutralizing titer was calculated as the inverse of the highest neutralizing dilution.

Histopathologic analysis

Organs Paraffin blocks were processed in serial sections for hematoxylin and eosin (HE) staining and control slides (Gill's n°1 hematoxylin, Sigma; Eosin Y acqueous 0.5% VWR international, Rosny-sous-Bois, France). In addition, Luxol fast blue and Von Kossa staining were performed on fetal brain slides. Histological analysis included recording and semiquantitative grading of the overall severity of the main lesions. Different sampling was initiated from the basal plate through the chorionic villi and chorionic plate in order to obtain the most homogeneous results. Furthermore, according to the lesion appearance, the histopathological analysis considered two subdivisions of lesion component: severity/type of inflammation and degeneration (edema, necrosis)/cellular loss. For each lesion, a score ranging from 0 to 4 depending on the subjective severity of the lesion was proposed (0 = not present, 1 = mild degree, 2 = moderate degree, 3 = high degree, 4 = intense degree). For placenta, sampling was initiated from the basal plate through the chorionic villus and chorionic plate and the sum of the scores for each lesion was calculated (Fig. 8).

Results

Study plan and pregnancy outcome

Four cynomolgus macaque fetuses were intramuscularly inoculated by a trans-amniotic echo-guided procedure at the beginning of the second third of pregnancy with 1×10^3 pfu of a French Polynesian ZIKV strain (H/PF/13). Two other fetuses were sham inoculated. Thereafter, the dam/fetus pairs were subjected to frequent sample collection and monitoring, as shown in Fig. 1. No inoculation-related complications were noted, and in particular, there was no rupture of membranes or fetal death. Cesarean delivery and fetal euthanasia were performed either 1 month after intramuscular ZIKV inoculation in three pairs or a few days before term for the other three pairs (2 ZIKV-exposed individuals and 1 mock-exposed individual per group). None of the dams showed clinical signs of Zika infection, and all the dams remained afebrile during the study period; infected dams were euthanized 1 month after cesarean section. Weights and hemograms did not show any pathological variation compared to those of the 2 mock-exposed pairs (data not shown).

Maternal viral load

Four days post fetal inoculation (dpfi), the virus was detectable at significant levels in the blood of only 2 out of the 4 dams. In the other two exposed dams, the viremia on day 4 either remained below the lower limit of quantification (CA872B) or was detected only later (BZ514 viremia starting 1 week after fetal exposure) (Fig. 2). Thereafter, plasma viremia was detectable up to 20–40 dpfi in all 4 dams. The viremia peaked between days 4 and 10 (mean 7 dpfi), which differs from the reported data of subcutaneous inoculation in dams (usually before 5 dpi) [13]. Thus, compared to the results of previous trials conducted in our laboratory, the duration and intensity of ZIKV infection are much greater in pregnant females than in adult animals [33]. All dams had detectable viral loads in their saliva between 4 and 10 dpfi that peaked close to the time of viremia (BZ514 and CA872B) after 2 days for the animal BB807C, but that of CA953D remained below the lower limit of quantification. None of these four animals had a detectable viral load in their vaginal fluids (data not shown).

Overall, the detection of maternal viremia suggests retrograde transmission from the fetus to the mother through the placental barrier, considering that retrograde transmission via a non-hematogenous route seems highly

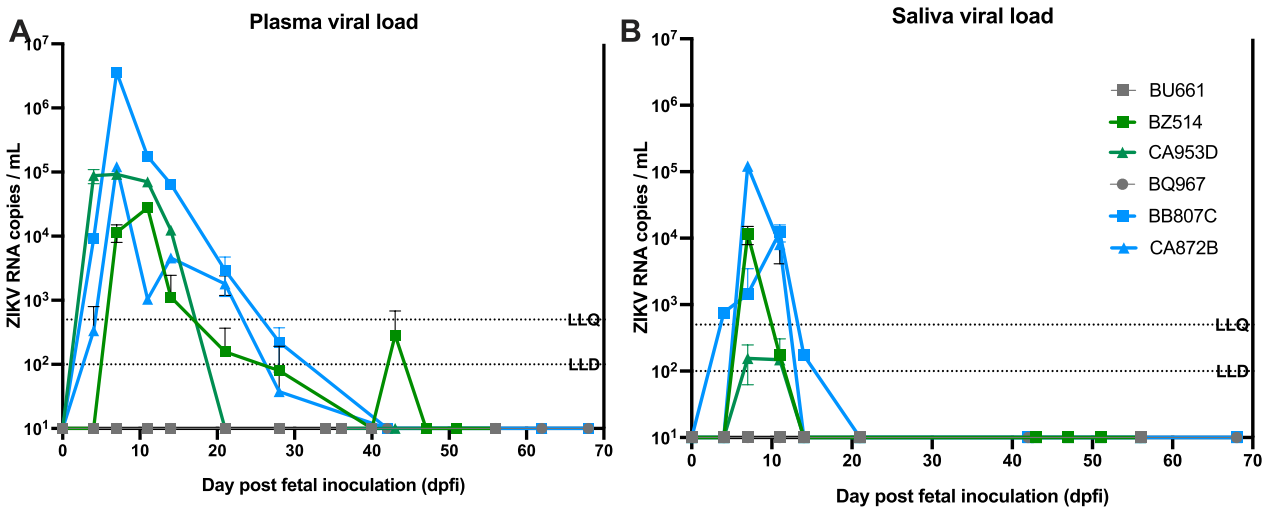

Fig. 2 Viral load and shedding of ZIKV in dams following in utero exposure of the fetus. **A**: Plasma viremia, **B**: saliva viral load. Viral loads were determined on days 4, 7, 11, 14, 21, 28, 34–40, 42, 43–51, 56, 62, and 68. An RT—qPCR assay was used to measure ZIKV RNA loads, reported as log 10 ZIKV copies/mL. LLD: Lower limit of detection. LLQ: lower limit of quantification

improbable given the pathogenicity associated with ZIKV.

The persistence of the viral RNA in the blood, fluid, lymphoid tissue and central nervous system was also assessed at 1 month after the cesarean section (Supplementary Table 1). We did not detect any viral RNA in the blood or fluids, but we detected viral RNA in the spleens of the two females at 34–36 dpfi (BZ514 and CA953D, 194.7 and 0.3 RNA copies/mg, respectively)that were euthanized 60 dpfi (Group 1). But we did not detect viral RNA in the spleen of the mothers that were euthanized at 90 dpfi (Group 2). However, in animal BZ514 (Group 1, euthanized at 56 dpfi), viral RNA was detectable in the iliac and inguinal lymph nodes (77.4 and 71 RNA copies/mg, respectively), and in animal BB807C (Group 2, euthanized at 98 dpfi), viral RNA was detectable in the nasopharyngeal and axillary lymph nodes (55.7 and 14.4 RNA copies/mg, respectively).

Ultrasound and fetal biometrics

Ultrasound assessment was conducted weekly to monitor fetal viability and growth and to detect any cerebral defects. Head circumference was compared to femur length, which was assumed not to be impacted by ZIKV [34].

Whereas no major fetal defects were found, a tendency towards a reduction in cephalic perimeter has been observed in all infected fetuses. However, the observed perimeter reduction was less than the value recognized as characteristic of microcephaly (<2 SD, as shown in Fig. 3). All mock-exposed fetuses had normal biometrics for cephalic perimeter and femur length.

Fetal viral load

An amniotic fluid puncture was performed before fetal extraction for euthanasia (i.e., 35 dpfi for group 1 and 70 dpfi for group 2). Only the sample from CA953D-f (group 1) had a detectable viral load in the amniotic fluid, while its experimental duplicate (ie BZ514-f, infected fetuses for wich amniocentesis was performed 1 month after ZIKV inoculation) was negative, as were the samples from the two fetuses extracted at 2 months postexposure.

As expected, fetuses euthanized 1 month after inoculation (CA953D-f and BZ514-f) had high levels of ZIKV RNA in brain and placental tissues (Fig. 4A) that were largely above the quantification threshold (2 copies/ng total RNA), except in the brainstem and lumbar spinal cord of CA953D-f. Importantly, the number of infected tissues was lower at 2 months postexposure than at 1 month postexposure ($p < 0.001$ chi-square test). In addition, the viral loads in tissues from fetuses euthanized before natural delivery (CA872B-f, BB807C-f) were lower than those observed at month one postinoculation, despite the small persistence of the virus in the cerebral parenchyma and apparent increase in the placenta and amnios (Fig. 4B). Thus, out of the 38 ZIKV-positive tissues tested in the 2-month fetal group, only 6 had ZIKV-positive signal, while 31/38 had ZIKV-positive genomic material in the 1-month fetal group (Fig. 4A). Overall, these data suggest that the viral load is controlled during pregnancy.

Cytokine profiles

The cytokine response was variable between dams (Fig. 5). There was no evidence of differences in the

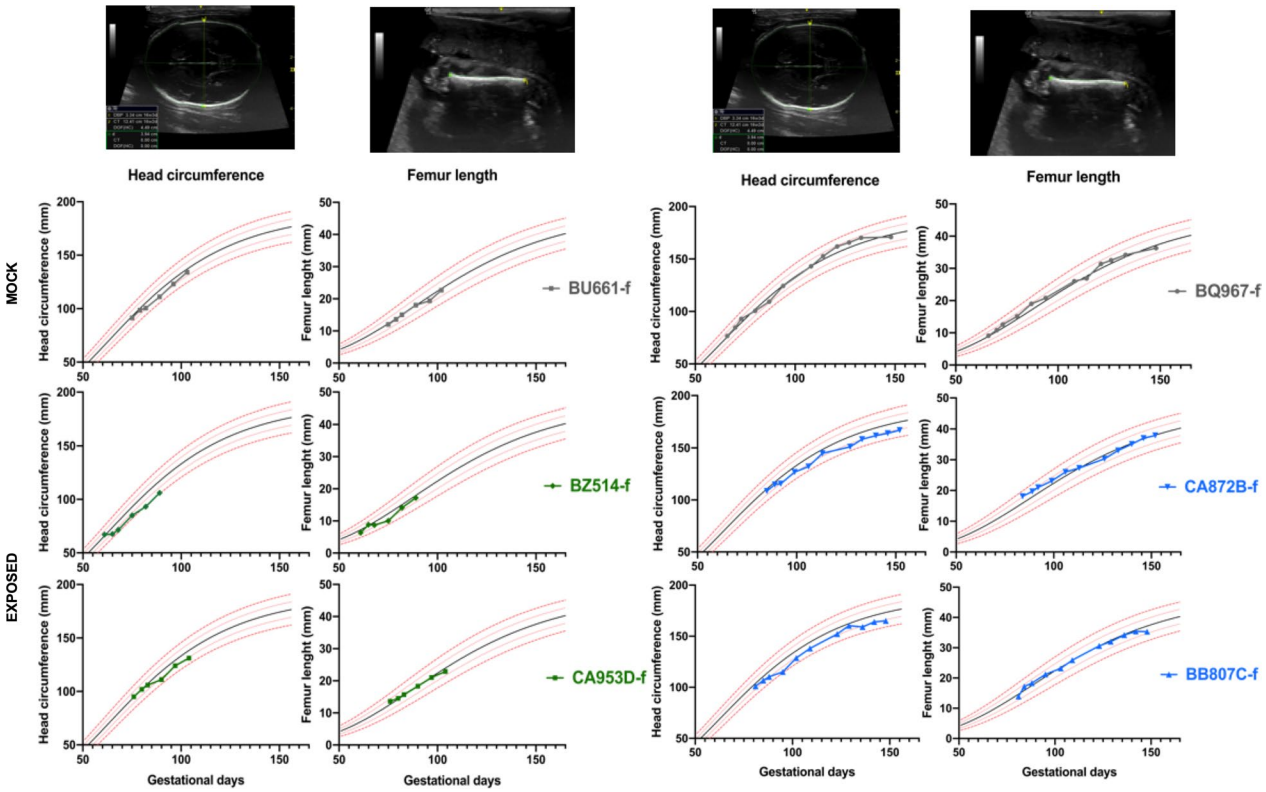

Fig. 3 Fetal ultrasound biometrics. Serial ultrasound biometrics, including head circumference and femur length, were performed during gestation. Reference ranges were plotted and fit using nonlinear regression with data from Tarantal et al. [26]. The black line represents the mean value, and the red line represents the standard deviation. On the left: group 1 euthanized 1 month post inoculation included: BU661-f, BZ514-f and CA953D-f. On the right: group 2 euthanized 2 months post inoculation included: BQQ967-f, CA872B-f and BB807C-f. The time of the first ultrasound measurement was also the day of virus (or mock) inoculation

protein profiles between infected and mock dams. BB807C (infected group 2, subjected to cesarian section before term, i.e., 2 months after fetal inoculation) had frequently the highest levels, especially in GM-CSF, IFNγ, IL4, IL13, IL1β, IL6, IL15, and TNFγ. However, since the clinical, ultrasound and viral load profiles were similar between the different dams and fetuses, it was not possible to draw any conclusions. Conversely, BQ967 (mock) frequently had the lowest levels, often below the detection limit, especially for IL5, IL12-23, IFNγ, IL4, IL13, MIP1α, IL1β, IL6, IL15, TNFα, VEGF and IL2. However, the other mock infected animal BU661 had high levels of IL12-23, MIP-1β, MIP-1α, IL-8, and IL-2. Interestingly, for the mother BZ514, at approximately day 40 post inoculation, the expression of IL5, IL12-23, IFNγ, IL4, MIP1α, IL1b, TNFα, IL8, VEGF, IL2 and IL10 increased, corresponding to the reappearance of ZIKV in the maternal blood but being below the limit of virus quantification (Fig. 2). The effect of cesarean section and removal of the infected fetus did not lead to any difference in cytokine kinetics between the two groups.

Maternal serology

To determine the humoral immune response of the mothers, the ratio of OD (rOD), the seroneutralization titer at all dpfi, and the anti-ZIKV IgG titers at some dpfi were determined (Fig. 6). All the profiles were very similar, confirming the pertinence of the kinetics observed following rDO using 1/500 dilutions of serum (Fig. 6A). Thus, the appearance, maximum and disappearance of neutralizing IgG can be observed and compared.

Using serum samples diluted 1/500, we investigated the kinetics of specific anti-ZIKV IgG against inactivated ZIKV in the six dams by ELISA (Fig. 6). None of the mock dams recognized inactivated ZIKV, while every infected dam presented an anti-ZIKV IgG signal that became detectable either at 14 dpfi (BB807C and CA872B) or between 14 and 21 dpfi (BZ514 and CA953D), as shown in Fig. 6A.

The increase in anti-ZIKV IgG levels was identical for the 4 dams and ended at approximately 40 dpfi; subsequently, the anti-ZIKV IgG levels decreased slightly in two dams (CA953D and CA872B; Fig. 6A). To assess the exact titer of these anti-ZIKV IgGs, we performed

A

			Group 1 34/36 days of infection			Group 2 68/70 days of infection		
			BU661-f	BZ514-f	CA953D-f	BQ967-f	BB807C-f	CA872B-f
Placenta and amnios	Placenta	Maternal side	0	44	485	0	0	0
		Fœtal side	0	0	432	0	0	2699
		Middle	0	11	0	0	0	0
	Amnios		0	1223	13	0	13149	33774
Central nervous system	Frontal	Cortex	0	2205	1194	0	0	0
		White matter	0	1483	0	0	0	0
	Parietal / temporal	Cortex	0	1448	227	0	0	1758
		White matter	0	216	21	0	0	0
		Basal Nuclei	0	76	27	0	0	0
	Occipital	Cortex	0	22323	12	0	98	0
		White mater	0	638	2069	0	591	0
	Brain Stem		0	83	2	0	0	0
	Cerebelum		0	35	9	0	0	0
Spinal Cord	Cervical		0	36	0	0	0	0
	Thoracic		0	64	0	0	0	0
	Lumbar		0	290	1	0	0	0
Abdominal organs	Thymus		0	0	8	0	0	0
	Liver		0	0	29	0	0	0
	Spleen		0	15	28	0	0	0

Background colors: < 100 copies/ng. 100 copies/ng to 1000 copies/ng. > 1000 copies/mg.

B

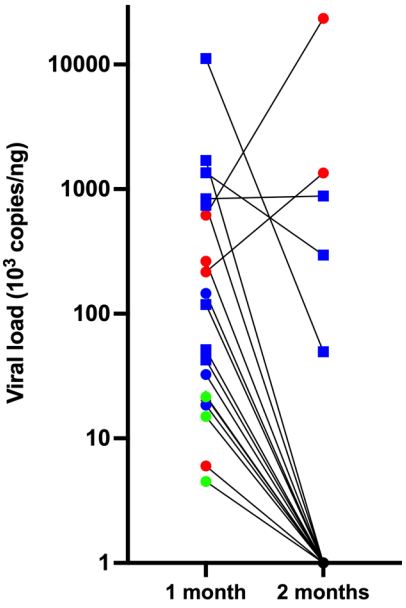

Fig. 4 Fetal tissue viral loads. **A**: Total RNA was isolated from tissues after euthanasia and is presented as ZIKV RNA/ng total RNA. **B**: Comparison of fetal tissue viral loads (mean for each time) according to the duration of exposure to ZIKV. Blue: nervous tissues; red: placental tissues; green: liver, spleen and thymus

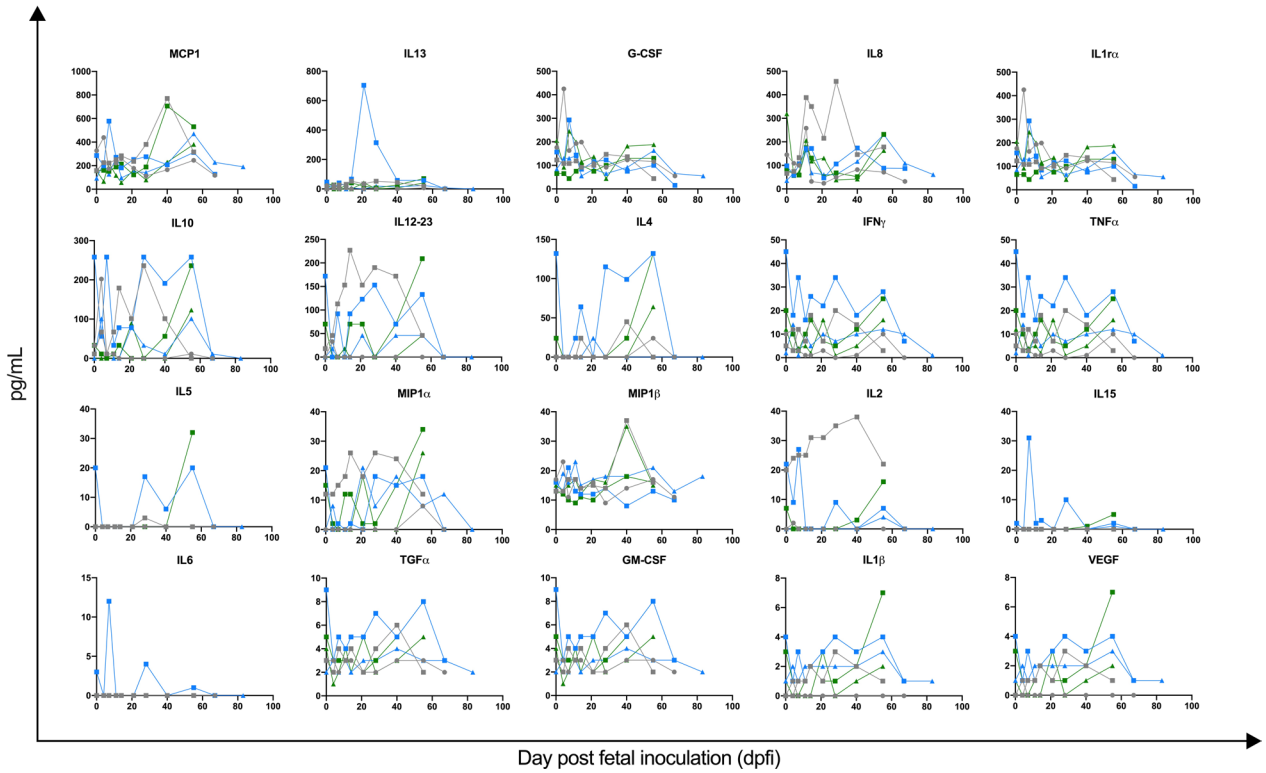

Fig. 5 Maternal plasma cytokine and chemokine levels in response to fetal ZIKV inoculation. All infected dams are represented, and each point represents a value. Green (group 1; square BZ514, triangle CA953D), blue (group 2; square BB807C, triangle CA872B), gray (mock exposed; square BU661, circle BQ967)

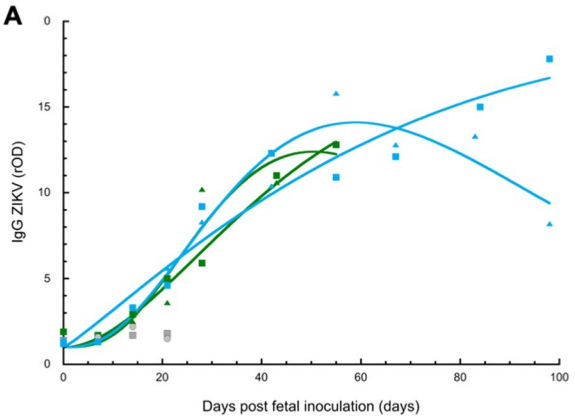

B

Female	dpfi 21	dpfi 55	dpfi 98
BB807C	1/4000	1/32000	1/32000
CA872B	1/4000	1/32000	1/16000
BZ514	1/2000	1/8000	ND
CA953D	1/2000	1/16000	ND

Fig. 6 **A**: Kinetics of specific anti-ZIKV IgG antibodies in the sera of dams after fetal ZIKV infection (blue and green dots). The curves are mathematical models of the evolution of IgG levels (Wood equation [35]). Specific antibody levels are expressed as the rOD of IgG detection in 1/500 diluted sera against whole-lysed ZIKV from mock-producing cells. The ratio of mock-infected dam sera (gray dots) was 1, as expected, while the cutoff for positive detection was 3. Green (group 1; square BZ514, triangle CA953D), blue (group 2; square BB807C, triangle CA872B), gray (mock exposed; square BU661, circle BQ967). **B**: Table of anti-ZIKV IgG titers obtained by limiting dilution. ND: not done, dpfi = days post fetal inoculation

titration by limit dilution and found that the decrease in the anti-ZIKV IgG titer in CA872B was also observed from 1/32000 at dpfi 55 to 1/16000 at dpfi 98 (Fig. 6B); rDO had similar results as did the titer.

IgG functionality

Neutralization assays were performed for the four infected dams by incubating the sera with ZIKV (Table 1). The first sign of specific virus neutralization was observed with sera collected at dpfi 14 (for BZ514, BB807C and CA872B with titers of 1/20, 1/80 and 1/80, respectively) or dpfi 21 for CA953D (1/80). The maximum was reached at dpfi 28 for BZ514, BB807C and CA872B (1/320) and at dpfi 55 for CA953D (1/320). Notably, for the total anti-ZIKV IgG titer, there was a decrease in the neutralizing titer in the serum of the CA872B female.

Histology

In addition to hematoxylin and eosin (H&E) staining of brain slides, we performed luxol fast blue staining, which assesses myelination pathway activity, and Von Kossa staining, which assesses calcification; however, no histopathological changes can be observed in the nervous system of the exposed fetus compared to that in the mock-exposed fetus. All the images revealed that the brain tissues exhibited a normal pattern (supplementary Figs. S3 and S4).

Preterm placentas sampled at 34–36 dpf (CA953D and BZ514) on gestational days (GDs) 110 and 97, respectively, showed a few fibronectin-necrotic foci accompanied by some inflammatory cell infiltration in the villi. The infiltrations were composed mainly of polymorphonuclear neutrophils but also of macrophages, which are characterized by abundant cytoplasm, pale eosinophilic space and a large nucleus with a central nucleolus, and lymphocytes, which are small, round cells (Fig. 7A, B). These lesions were larger and easier to see in CA953D fetal tissue. In addition, CA953D presented a necrotic lesion on the side of the basal plate that looked like an infarction (well-delineated focal coagulation necrosis as observed for BB807C in Fig. 7B). Rare images suggest vasculitis lesions with excess fibrin and infiltred mononuclear cells around the vessels but without clear vascular lesions.

Table 1 Seroneutralization kinetics. Titers were obtained using the MN50 technique

dpfi/ID	0	7	14	21	28	42	55	67	84	98
BZ514	< 1/20	< 1/20	**1/20**	**1/80**	**> 1/320**	**1/40**	**1/160**	ND	ND	ND
CA953D	< 1/20	< 1/20	< 1/20	**1/80**	**1/40**	**1/160**	**> 1/320**	ND	ND	ND
BB807C	< 1/20	< 1/20	**1/80**	**1/80**	**> 1/320**	**> 1/320**	**> 1/320**	**> 1/320**	**1/160**	**> 1/320**
CA872B	< 1/20	< 1/20	**1/80**	**1/160**	**> 1/320**	**1/160**	**> 1/320**	**> 1/320**	**1/40**	**1/80**

Positive values are indicated in bold

ND not done, *dpfi* days post fetal infection

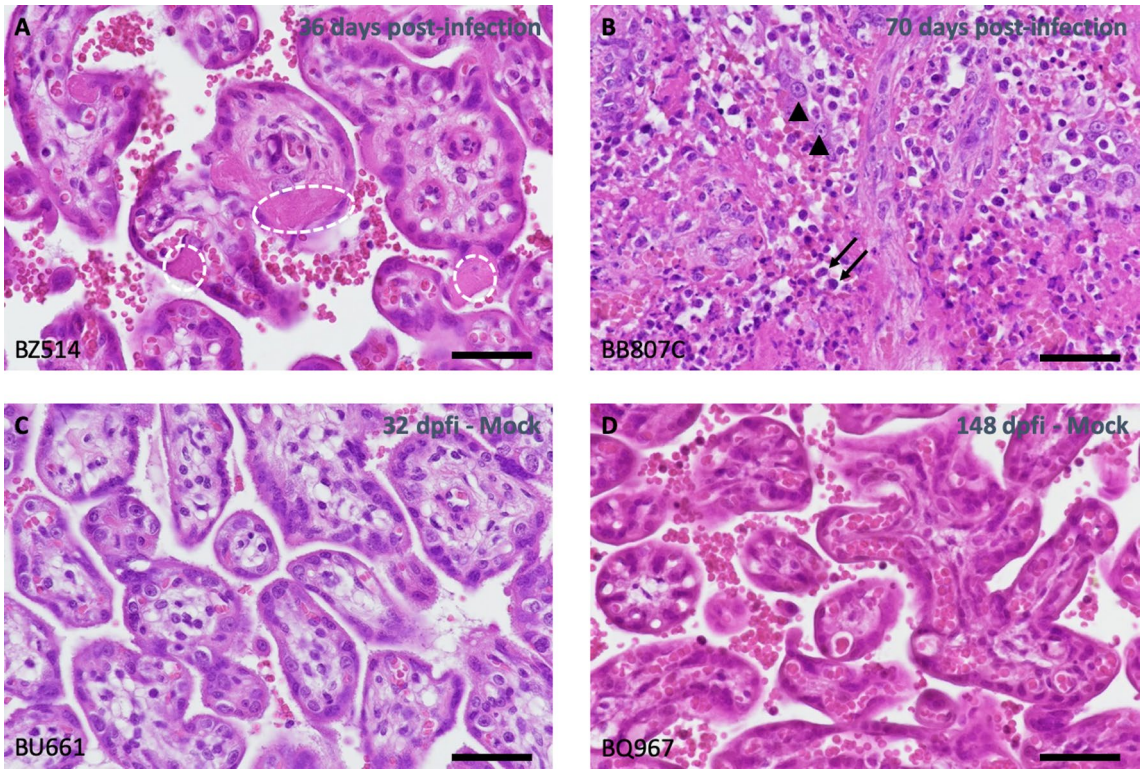

Fig. 7 Hematoxylin–eosin staining of placenta from infected and unexposed fetus/mother couples. **A** Fibrin plug and sceral fibrosis are observed in the villi. The histology score for this tissue was 3. **B** Multifocal focal cellular debris associated with fibrin (necrosis) and mixed neutrophilic, macrophagic and lymphocytic infiltration were observed with a histology score of 7 (Fig. 8). **C** and **D** Normal tissue was observed in control animals (histological score = 0). Doted circle (fibrin); PMN black arrow; Macrophage arrowhead. Scale Bar = 50 µm

In term placentas: The lesions are identical between the two couples that were sampled at 68–70 dpfi (CA872C and BB807C) on GD151-153 and lesions are present on approximately 5–10% of the villi, with images of villous sclerosis ± accumulation of fibrin in the villi. This is exemplified in Fig. 7B as white/pink trabeculae when compared to the control (Fig. 7D), in which the villi remained independently separated by a well-defined white space noncolapsed. This could be a sequela of lesions such as vasculitis to infection (Fig. 8).

The inflammatory status of the placenta was still observable in the uterus of the females we sampled 1 month after the caesarian section (Fig. S2). Lower level of histology score was observed in the mother to infant interface (uterus and vagina) but at an equivalent level between 1-month-old group (4, 1 and 1, 2 for uterus and vagina respectively for CA953 and BZ514) vs 2-month-old-group (3, 2 and 1, 2 for uterus and vagina respectively for CA872B and BB807C).

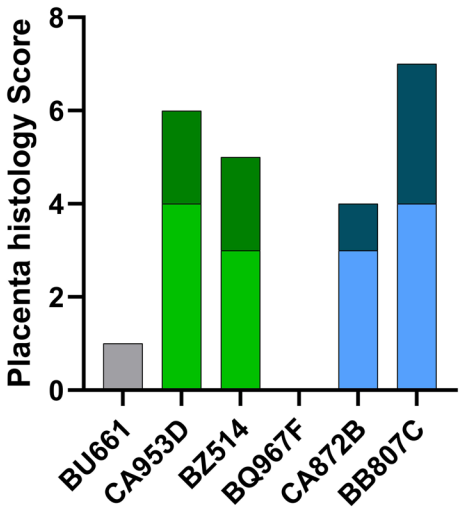

Fig. 8 Histological score of the placenta. Gray: mock-exposed pairs, green: 1-month-old group, blue: 2-month-old group. Lights colors represent inflammation score and dark colors represent degeneration score

Discussion

Validation of the fetal in utero *inoculation model*

The results from this study indicate that direct inoculation of the fetus via the intramuscular route is a good strategy for examining the fetal effects of ZIKV. To our knowledge, this is the first study conducted with exclusive fetal inoculation. Previously, Coffey et al. inoculated rhesus monkey dams with ZIKV via intravenous and intra-amniotic routes and found ZIKV RNA in many tissues as well as reduced neural precursor cells [20]. The limitations of the NHP animal model for congenital Zika syndrome include relatively low fetal damage (no macroscopic lesion apart from relative microcephaly), variable infection rates (between 50 and 100% of fetuses were infected after maternal inoculation), and a high risk of fetal death after maternal inoculation [36]. However, in a more recent study from the same group in which virus was inoculated subcutaneously into mothers at G45, no clinical or pathogenic signs or viruses were detected at delivery [37]. Following our fetal intramuscular inoculation, all the challenged dams and fetuses presented a viral load in the blood or tissues. Importantly, compared with control infection, ZIKV infection led to relative microcephalia in all infected fetuses. Direct intramuscular inoculation of the fetus via the intraamniotic route allows (1) maximization of the number of fetuses infected by the shunting placental barrier, (2) a trend toward smaller head circumference, and (3) the use of a low inoculum dose (1×10^3 pfu).

Ultrasound and fetal pathology

Observational studies of human cases revealed a rate of Zika-associated birth defects of approximately 5–7% after maternal Zika infection [38, 39]. The findings associated with the central nervous system (CNS) are microcephaly, ventriculomegaly, calcifications, malformations of cortical development, anomalies of the corpus callosum and of the posterior fossa, arthrogryposis, ocular abnormalities, and extraneurologic signs such as intrauterine growth restriction and placentomegaly [40]. ZIKV-related CNS anomalies present mainly as progressive CNS lesions and a slowing rate of fetal head growth, and these anomalies seem to be evident only in the late second trimester, even when maternal infection occurs in the first trimester [41].

No antenatal macroscopic lesions were found in NHP models of congenital ZIKV infection. A study by Steinbach et al. suggested that a reduction in head circumference assessed by ultrasound does not consistently predict a low brain mass (> −2 SD) in newborn NHPs after ZIKV infection, which is a potential limitation of prenatal imaging in identifying subtle brain changes in NHPs [19]. Microcephaly has been reported in mouse and swine models of gestational ZIKV infection, as has a reduction in the growth rate of the fetal head in NHP models [17, 18, 20, 42, 43]. Our in utero inoculation model made it possible to observe cerebral damage, which was defined by a reduction in the cephalic perimeter that can be visualized by ultrasound; this process was similar for all infected fetuses. Hematoxylin and eosin staining and Luxol fast blue and Von Kossa staining were performed on the fetal brains, and unfortunately, we could not correlate the ultrasound observations with patent histological changes in the nervous system (Figs. S3 and S4). In particular, we did not observe brain calcification, which is well described in the fetal brains of human newborns or stillborn neonates infected with Zika virus. A recent study described the potential role of a recent acquired deletion (2016) in the glycan loop of the E protein within Asian ZIKV strains in increasing neurotropism and subsequent brain damage; however, our ZIKV strain from 2013 did not harbor this deletion [44].

Our results are thus consistent with the data in the literature, given (1) moderate encephalic damage, (2) slower growth of the fetal head during pregnancy, and (3) no other detectable macroscopic damage.

In a Brazilian study, despite high specificity, ZIKV-associated abnormalities detected by prenatal ultrasound poorly predicted neonatal outcome, suggesting ultrasound is a poor diagnostic tool for congenital Zika syndrome [45]. The definition of microcephaly remains controversial, typically between −2 SD and −3 SD below the median. However, sonographic recognition of a normally proportioned fetus may help exclude a broader spectrum of ZIKV-associated congenital injuries detected postnatally [34]. Ultrasound lesions are only part of congenital Zika syndrome, and some lesions may become visible only later, even if the fetus appears asymptomatic at birth. Our model is valuable as it reliably reproduces fetal Zika infection pathogenesis without visible macroscopic damage.

Fetal and dam viral loads

The timing of infection and its impact on fetal transmission remain difficult to establish. In our study, all the dams exhibited viremia after in utero exposure. Maternofetal transmission of ZIKV is estimated to occur in 20–30% of infected pregnant women in human clinical studies [39, 46, 47] and 50–70% of infected pregnant female in nonhuman primate preclinical studies [9, 13, 17–20, 48]. According to our model, retrograde vertical transmission occurred in 100% of cases. Since close to full clearance of the virus just before delivery is observed despite direct inoculation, our study suggested that the rate of maternal transmission of ZIKV would be much greater than that reported in other studies. Clearance of

ZIKV in amniotic fluid and fetal blood has previously been shown in infected fetuses, but control in the brain has never been clearly demonstrated [49]. Earlier work in a rhesus macaque model from which some ZIKV mutants were isolated from brain tissues shown an increased neurovirulence of these "adapted strain" when intracranially inoculated in mice. But these indirect findings could not be reproduced in later studies [50, 51]. Fetal pathology occurs in humans and multiple animal models even in the absence of ZIKV detection in the fetus's body [45, 49]. In addition to the indirect effects of maternal ZIKV infection on the developing fetus, partly because of placental function impairment [52], we suggest that transient fetal ZIKV infection is sufficient to cause brain damage.

Our results suggest that the absence of ZIKV RNA in fetal tissue at term, as observed in some cases, does not necessarily indicate the absence of maternofetal transmission or fetal infection. Crooks et al., after inoculating pregnant rhesus macaques at the end of the first trimester, reported a significant difference in viral load and pathology at the maternal-to-fetal interface but not at the fetal level and found no evidence of vertical ZIKV transmission at delivery [53]. In a recent paper, intravaginal inoculation at early stage (GD30) of a high dose of African ZIKV in pregnant macaques induced fetal loss 2 weeks later in 2 out of 3 dams, during which ZIKV was detected in all tissues; at term, ZIKV was detected only at the maternal–fetal interface [54]. In light of our results, transient fetal infection may also have occurred. However, in contrast to Crooks et al., our direct fetal inoculation allowed macroscopic cerebral damage [53].

In our study, in contrast to the findings of the preliminary study by Steinbach et al. [19], no correlation could be demonstrated between extended viremia and adverse fetal outcomes. All the dams had extended viraemia, and a reduction in the cephalic perimeter was observed in all the fetuses, although we could observe clearance of ZIKV during gestation in fetal tissues.

While all fetuses were directly infected, maternal viremia was prolonged in all fetuses, even in group 2, in which fetuses were euthanized at term with almost no virus in the brain. However, the viral load in the placenta and amnios persists to a significant degree, suggesting that the placenta is the reservoir of the virus for this prolonged viremia rather than the fetus itself. In addition, the placenta of the infected dams showed inflammatory lesions associated with vascular changes (villous sclerosis and placental infarction). It is therefore likely that these changes could be the cause of the brain diameter reduction. Although Magnani et al. did not find de novo mutations in intrahost ZIKV populations associated with viral replication in the amniotic fluid of 11 pregnant rhesus macaques, recent work has shown that selection of mutations may occur specifically in the placenta of pregnant rhesus macaques (those with a mutation in the NS2B protein) but only in 50% of the tested couples [48, 55]. This might be consistent with the large variation we observed between the fetuses extracted at 2 months post-inoculation. Finally, within the rhesus model, ZIKV pathogenesis was clearly enhanced. A new study focusing on the African lineage of ZIKV, which inoculated the virus in mothers earlier than in our study (GD 30/45 versus GD 60/85), revealed extensive infection of fetal interface tissues on day 7 post-inoculation (pi), persisting and increasing on day 14 pi, along with infection of fetal tissues and fluids [24]. In this assay, the virus reached the fetus in 8 out of 9 mothers, confirming the major role played by placental/decidua tissues in enhancing virus replication, as observed in our study.

Immune response to control fetal infection

During the acute phase, it was often observed that ZIKV elicited rapid increase in serum cytokines and chemokines. This was shown specifically in a macaque model for IFNα, TNFα, MCP-1, IL-15, IL-10, IL1RA, and MIP-1α after exposure to 5 10^6 pfu of ZIKV, with responses peaking at approximately 1–2 days post infection [56]. The systemic cytokine response was minimal after subcutaneous ZIKV inoculation of rhesus macaques in the study by Hirsch et al. [57]. The in utero ZIKV infection route with 10^3 pfu elicited both a delayed viral peak and delayed cytokine and chemokine responses (as an example, peak on day 7 or day 40 for MCP-1), in contrast to direct peripheral infection of adult macaques. However, perhaps due to the unique immunotolerance context related to pregnancy and the low dose of virus inoculated, differences in cytokine and chemokine responses between pregnant and mock-exposed animals are unclear due to the small sample size and large variation [58].

Cytokine expression in the plasma did not change following infection or clearance of the viral reservoir (i.e., after cesarean section in our animals). One hypothesis is that this results from direct inhibition of innate immune pathways by ZIKV that direct the synthesis and secretion of proinflammatory cytokines [59].

Despite robust maternal anti-ZIKV-specific antibody responses, ZIKV RNA was still detected in tissues from all animals. Similarly, Nguyen et al. [18] detected ZIKV in the peripheral blood of pregnant NHPs for a much longer period (up to 43 days) than was observed in adult male macaque and nonpregnant female [60, 61] (5 days). All the neutralizing antibodies were detectable from 14 or 21 dfpi; simultaneously, all the neutralizing antibodies were detectable via ELISA and reached their maximum at 28 dfpi, except for one monkey (Table 1). The antibody kinetics were comparable to those leading to high titers found

at 30 days post infection in nonpregnant rhesus monkeys by Pantoja et al. and comparable with those in pregnant human women [62, 63]. Notably, however, seroneutralization occurred later than that observed in Haddow et al., who exposed animals through vaginal or rectal routes [64].

In animals from the 1-month group, the viral load in BZ514-f was greater than that in CA953D-f, i.e., 22 323 virus copies per ng of total RNA in the cortex occipital lobe versus 12, respectively. In their mothers, the IgG titer was 1/8000 versus 1/16000 at 55 dpf; moreover, seroneutralization decreased for BZ514 but not for CA953D, with an effect on the fetuses' head circumference that was smaller for BZ514-f than for CA953D-f.

In the 2-month group, the same tendency was found for the CA872B-m/f and BB807C-m/f pairs, with the highest viral load for CA872B-f compared with BB807C-f (33,774 vs 13,149 in amnios, respectively); however, in the mothers, we found a lower IgG titer at dpfi 98 (1/16000 in CA872B versus 1/32000 in BB807C), a low seroneutralization titer at dpfi 98 (1/80 versus 1/320) and a smaller head circumference for CA972B-f than for BB807C-f.

For both groups, the observations were similar: the highest viral load was associated with a faster decrease in the IgG titer and a lower degree of seroneutralization in association with the smallest head circumference. Here, we correlated the immunological response, viral load and pathological effect on the fetus.

Limitations of our study

Our study demonstrated that viral load was controlled at the brain level despite the persistent presence of the virus in the placenta. Due to limitations in longitudinally tracking fetal viral load, this inference is drawn from higher viral loads observed in fetuses delivered earlier post-infection, suggesting the potential for viral clearance. Due to the small number of subjects, it is difficult to compare the different groups statistically, especially with respect to the immune response. Furthermore, in the absence of immunohistochemistry or in situ hybridization analysis, our understanding of histological lesions is restricted to qualitative analysis. We have not examined the genetic characteristics of the viruses detected in the tissues or explored their replicative capacity, which was outside the objective of this work but deserves further exploration to obtain further insight into the role of the placenta. Characterization of fetal involvement by analysis of RNA profile expression and investigations at the molecular level during pregnancy would provide a better characterization of the disease.

Conclusions

ZIKV infection during the early step of fetal development induces brain disease, but most of the virus is cleared before delivery. This may explain the relatively high percentage of subclinical disease at birth without abrogation of induced sustained long-term neurocognitive impairment. Thus, in humans, many children from ZIKV-infected mothers are apparently born within the normal range without microcephaly, during which time their development changes.

Abbreviations

ZIKV	Zika virus
RT-qPCR	Quantitative reverse transcription polymerase chain reaction
PMA	Phorbol 12-myristate 13-acetate
Pfu	Plaque forming unit
PBMC	Peripheral blood mononuclear cell
rOD	Optical density
NHP	Non-human primate
LPS	Lipopolysacharid
IgG	Immunoglobulin G
GD	Gestation day
GAPDH	Glyceraldehyde 3-phosphate dehydrogenase
ELISA	Enzyme linked immuno sorbent assay
EDTA	Ethylen diamine tetra-acetic acid
Dpfi	Day post fetal infection
Dpe	Day post exposure

Supplementary Information

The online version contains supplementary material available at https://doi.org/10.1186/s12985-024-02468-x.

Supplementary Material 1

Acknowledgements

IDMIT L2I platform: Julie Morin; Animal Healthcare IDMIT Francis Relouzat, Julien Lemaitre, Joanna Demilly. External review: Georges Snounou. Antibody measurements were obtained from Laurent Bosio, Manon Geulen and Bernard Tenebray.

Author contributions

Conceptualization, Pierre Roques; Data curation, Charles Egloff, Jessica Denis, Nathalie Bosquet, Cyril Badaut and Pierre Roques; Formal analysis, Charles Egloff, Cyril Badaut and Pierre Roques; Funding acquisition, Roger Le Grand and Pierre Roques; Investigation, Charles Egloff, Claire-Maëlle Fovet, Jessica Denis, Quentin Pascal, Laetitita Bossevot, Marco Léonec and Guillaume Durand; Methodology, Roger Le Grand, Olivier Picone and Pierre Roques; Resources, Nathalie Bosquet, Cyril Badaut, Isabelle Leparc-Goffart and Pierre Roques; Supervision, Olivier Picone and Pierre Roques; Validation, Pierre Roques; Visualization, Charles Egloff; Writing—original draft, Charles Egloff, Claire-Maëlle Fovet and Pierre Roques; Writing—review and editing, Charles Egloff, Cyril Badaut and Pierre Roques.

Funding

This research was funded by the European Union H2020 program ZIKAlliance (grant number 734548). C.E. was supported by ARS Ile-de-France, grant number 2020–10.

Availability of data and materials

All data are presented in the manuscript

Declarations

Ethics approval and consent to participate

NHPs were housed in IDMIT infrastructure BSL3 facilities (CEA, Fontenay-aux-Roses, France) in accordance with French national regulations (Authorization number #D92-032-02 for animal use). The CEA used the ETS123 recommendations of the European Directive 2010/63/CE and the Standards for Human Care and Use of Laboratory Animals (Animal Welfare Assurance, OLAW number #A5826-01). All the studies were approved by the institutional ethical committee (CEtEA #44) authorization A16-050 and the Animal Welfare

Body (SBEA) authorization for amendment A20-021 (June 20, 2020) of the Commissariat à l'Energie Atomique (CEA) and were authorized by the French Research, Innovation and Education Ministry under registration number APAFIS#6805-20160920 171672 v4.

Consent for publication
All authors have read the manuscript and agree to publication.

Competing interests
The authors declare no conflict of interest. The funders had no role in the design of the study; in the collection, analyses, or interpretation of the data; in the writing of the manuscript; or in the decision to publish the results.

Received: 18 December 2023 Accepted: 13 August 2024
Published online: 03 September 2024

References

1. Dick GWA, Kitchen SF, Haddow AJ. Zika virus. I. Isolations and serological specificity. Trans R Soc Trop Med Hyg. 1952;46(5):509–20.
2. Adams Waldorf KM, Rubens CE, Gravett MG. Use of nonhuman primate models to investigate mechanisms of infection-associated preterm birth. BJOG. 2011;118(2):136–44.
3. Hcini N, Kugbe Y, Rafalimanana ZHL, Lambert V, Mathieu M, Carles G, et al. Association between confirmed congenital Zika infection at birth and outcomes up to 3 years of life. Nat Commun. 2021;12(1):3270.
4. Agarwal S, Scher MS. Fetal-neonatal neurology program development: continuum of care during the first 1000 days. J Perinatol. 2022;42(2):165–8.
5. Nakayama E, Kawai Y, Taniguchi S, Hazlewood JE, Shibasaki KI, Takahashi K, et al. Embryonic stage of congenital Zika virus infection determines fetal and postnatal outcomes in mice. Viruses. 2021;13(9):1807.
6. Narasimhan H, Chudnovets A, Burd I, Pekosz A, Klein SL. Animal models of congenital zika syndrome provide mechanistic insight into viral pathogenesis during pregnancy. PLoS Negl Trop Dis. 2020;14(10): e0008707.
7. Ades AE, Soriano-Arandes A, Alarcon A, Bonfante F, Thorne C, Peckham CS, et al. Vertical transmission of Zika virus and its outcomes: a Bayesian synthesis of prospective studies. Lancet Infect Dis. 2021;21(4):537–45.
8. Giakoumelou S, Wheelhouse N, Cuschieri K, Entrican G, Howie SEM, Horne AW. The role of infection in miscarriage. Hum Reprod Update. 2016;22(1):116–33.
9. Dudley DM, Van Rompay KK, Coffey LL, Ardeshir A, Keesler RI, Bliss-Moreau E, et al. Miscarriage and stillbirth following maternal Zika virus infection in nonhuman primates. Nat Med. 2018;24(8):1104–7.
10. van der Eijk AA, van Genderen PJ, Verdijk RM, Reusken CB, Mögling R, van Kampen JJA, et al. Miscarriage associated with Zika virus infection. N Engl J Med. 2016;375(10):1002–4.
11. Liang B, Guida JP, Costa Do Nascimento ML, Mysorekar IU. Host and viral mechanisms of congenital Zika syndrome. Virulence. 2019;10(1):768–75.
12. Li M, Brokaw A, Furuta AM, Coler B, Obregon-Perko V, Chahroudi A, et al. Non-human primate models to investigate mechanisms of infection-associated fetal and pediatric injury, teratogenesis and stillbirth. Front Genet. 2021;12:680342.
13. Martinot AJ, Abbink P, Afacan O, Prohl AK, Bronson R, Hecht JL, et al. Fetal neuropathology in Zika virus-infected pregnant female rhesus monkeys. Cell. 2018;173(5):1111-1122.e10.
14. Christian KM, Song H, Ming G. Pathophysiology and mechanisms of Zika virus infection in the nervous system. Annu Rev Neurosci. 2019;42:249–69.
15. Ausderau K, Kabakov S, Razo E, Mitzey AM, Bach KM, Crooks CM, et al. Neonatal development in prenatally Zika virus-exposed infant macaques with dengue immunity. Viruses. 2021;13(9):1878.
16. Koenig MR, Razo E, Mitzey A, Newman CM, Dudley DM, Breitbach ME, et al. Quantitative definition of neurobehavior, vision, hearing and brain volumes in macaques congenitally exposed to Zika virus. PLoS ONE. 2020;15(10):e0235877.
17. Adams Waldorf KM, Stencel-Baerenwald JE, Kapur RP, Studholme C, Boldenow E, Vornhagen J, et al. Fetal brain lesions after subcutaneous inoculation of Zika virus in a pregnant nonhuman primate. Nat Med. 2016;22(11):1256–9.
18. Nguyen SM, Antony KM, Dudley DM, Kohn S, Simmons HA, Wolfe B, et al. Highly efficient maternal-fetal Zika virus transmission in pregnant rhesus macaques. PLoS Pathog. 2017;13(5): e1006378.
19. Steinbach RJ, Haese NN, Smith JL, Colgin LMA, MacAllister RP, Greene JM, et al. A neonatal nonhuman primate model of gestational Zika virus infection with evidence of microencephaly, seizures and cardiomyopathy. PLoS ONE. 2020;15(1): e0227676.
20. Coffey LL, Keesler RI, Pesavento PA, Woolard K, Singapuri A, Watanabe J, et al. Intraamniotic Zika virus inoculation of pregnant rhesus macaques produces fetal neurologic disease. Nat Commun. 2018;9(1):2414.
21. Gurung S, Reuter N, Preno A, Dubaut J, Nadeau H, Hyatt K, et al. Zika virus infection at mid-gestation results in fetal cerebral cortical injury and fetal death in the olive baboon. PLoS Pathog. 2019;15(1): e1007507.
22. Newman CM, Tarantal AF, Martinez ML, Simmons HA, Morgan TK, Zeng X, et al. Early embryonic loss following intravaginal Zika virus challenge in rhesus macaques. Front Immunol. 2021;12:1835.
23. Koenig MR, Mitzey AM, Zeng X, Reyes L, Simmons HA, Morgan TK, et al. Vertical transmission of African-lineage Zika virus through the fetal membranes in a rhesus macaque (Macaca mulatta) model. PLoS Pathog. 2023;19(8):e1011274.
24. Koenig MR, Mitzey AM, Morgan TK, Zeng X, Simmons HA, Mejia A, et al. Infection of the maternal-fetal interface and vertical transmission following low-dose inoculation of pregnant rhesus macaques (Macaca mulatta) with an African-lineage Zika virus. PLoS ONE. 2023;18(5):e0284964.
25. Baronti C, Piorkowski G, Charrel RN, Boubis L, Leparc-Goffart I, De Lamballerie X. Complete coding sequence of Zika virus from a french polynesia outbreak in 2013. Genome Announc. 2014;2(3):e00500-e514.
26. Tarantal AF. Ultrasound imaging in Rhesus (Macaca Mulatta) and long-tailed (Macaca fascicularis) macaques. Reproductive and Research Applications. The Laboratory Primate. 2005;317–52.
27. Lanciotti RS, Kosoy OL, Laven JJ, Velez JO, Lambert AJ, Johnson AJ, et al. Genetic and serologic properties of Zika virus associated with an epidemic, Yap State, Micronesia, 2007. Emerg Infect Dis. 2008;14(8):1232–9.
28. Labadie K, Larcher T, Joubert C, Mannioui A, Delache B, Brochard P, et al. Chikungunya disease in nonhuman primates involves long-term viral persistence in macrophages. J Clin Invest. 2010;120(3):894–906.
29. Roques P, Fritzer A, Dereuddre-Bosquet N, Wressnigg N, Hochreiter R, Bossevot L, et al. Effectiveness of CHIKV vaccine VLA1553 demonstrated by passive transfer of human sera. JCI Insight. 2022;7(14):e160173.
30. Maisonnasse P, Guedj J, Contreras V, Behillil S, Solas C, Marlin R, et al. Hydroxychloroquine use against SARS-CoV-2 infection in non-human primates. Nature. 2020;585(7826):584–7.
31. Denis J, Attoumani S, Gravier P, Tenebray B, Garnier A, Briolant S, et al. High specificity and sensitivity of Zika EDIII-based ELISA diagnosis highlighted by a large human reference panel. PLoS Negl Trop Dis. 2019;13(9): e0007747.
32. Simonin Y, Loustalot F, Desmetz C, Foulongne V, Constant O, Fournier-Wirth C, et al. Zika virus strains potentially display different infectious profiles in human neural cells. EBioMedicine. 2016;12:161–9.
33. Zorrilla CD, García García I, García Fragoso L, De La Vega A. Zika virus infection in pregnancy: maternal, fetal, and neonatal considerations. J Infect Dis. 2017;216(suppl_10):S891–6.
34. Walker CL, Ehinger N, Mason B, Oler E, Little MTE, Ohuma EO, et al. Ultrasound prediction of Zika virus-associated congenital injury using the profile of fetal growth. PLoS ONE. 2020;15(5): e0233023.
35. Denis J, Garnier A, Claverie D, De Laval F, Attoumani S, Tenebray B, et al. The Wood equation allows consistent fitting of individual antibody-response profiles of Zika virus or SARS-CoV-2 infected patients. Heliyon. 2023;9(11): e21945.
36. Haese NN, Roberts VHJ, Chen A, Streblow DN, Morgan TK, Hirsch AJ. Nonhuman primate models of Zika virus infection and disease during pregnancy. Viruses. 2021;13(10):2088.
37. Dudley DM, Koenig MR, Stewart LM, Semler MR, Newman CM, Shepherd PM, et al. Human immune globulin treatment controls Zika viremia in pregnant rhesus macaques. PLoS ONE. 2022;17(7):e0266664.
38. Shapiro-Mendoza CK, Rice ME, Galang RR, Fulton AC, VanMaldeghem K, Prado MV, et al. Pregnancy outcomes after maternal Zika virus infection during pregnancy—U.S. territories, January 1, 2016-April 25, 2017. MMWR Morb Mortal Wkly Rep. 2017;66(23):615–21.
39. Pomar L, Vouga M, Lambert V, Pomar C, Hcini N, Jolivet A, et al. Maternal-fetal transmission and adverse perinatal outcomes in pregnant women

infected with Zika virus: prospective cohort study in French Guiana. BMJ. 2018;363:k4431.
40. Pomar L, Musso D, Malinger G, Vouga M, Panchaud A, Baud D. Zika virus during pregnancy: from maternal exposure to congenital Zika virus syndrome. Prenat Diagn. 2019;39(6):420–30.
41. Sarno M, Aquino M, Pimentel K, Cabral R, Costa G, Bastos F, et al. Progressive lesions of central nervous system in microcephalic fetuses with suspected congenital Zika virus syndrome. Ultrasound Obstet Gynecol. 2017;50(6):717–22.
42. Li C, Xu D, Ye Q, Hong S, Jiang Y, Liu X, et al. Zika virus disrupts neural progenitor development and leads to microcephaly in mice. Cell Stem Cell. 2016;19(5):672.
43. Wichgers Schreur PJ, van Keulen L, Anjema D, Kant J, Kortekaas J. Microencephaly in fetal piglets following in utero inoculation of Zika virus. Emerg Microbes Infect. 2018;7(1):42.
44. Cheng ML, Yang YX, Liu ZY, Wen D, Yang P, Huang XY, et al. Pathogenicity and structural basis of Zika variants with glycan loop deletions in the envelope protein. J Virol. 2022;96(23):e00879-e922.
45. Pereira JP, Nielsen-Saines K, Sperling J, Maykin MM, Damasceno L, Cardozo RF, et al. Association of prenatal ultrasonographic findings with adverse neonatal outcomes among pregnant women with Zika virus infection in Brazil. JAMA Netw Open. 2018;1(8):e186529.
46. Musso D, Ko AI, Baud D. Zika virus infection—after the pandemic. N Engl J Med. 2019;381(15):1444–57.
47. Conners EE, Lee EH, Thompson CN, McGibbon E, Rakeman JL, Iwamoto M, et al. Zika virus infection among pregnant women and their neonates in New York City, January 2016-June 2017. Obstet Gynecol. 2018;132(2):487–95.
48. Magnani DM, Rogers TF, Maness NJ, Grubaugh ND, Beutler N, Bailey VK, et al. Fetal demise and failed antibody therapy during Zika virus infection of pregnant macaques. Nat Commun. 2018;9(1):1624.
49. Schaub B, Vouga M, Najioullah F, Gueneret M, Monthieux A, Harte C, et al. Analysis of blood from Zika virus-infected fetuses: a prospective case series. Lancet Infect Dis. 2017;17(5):520–7.
50. Yuan L, Huang XY, Liu ZY, Zhang F, Zhu XL, Yu JY, et al. A single mutation in the prM protein of Zika virus contributes to fetal microcephaly. Science. 2017;358(6365):933–6.
51. Jaeger AS, Murrieta RA, Goren LR, Crooks CM, Moriarty RV, Weiler AM, et al. Zika viruses of African and Asian lineages cause fetal harm in a mouse model of vertical transmission. PLoS Negl Trop Dis [Internet]. avr 2019 [cité 21 oct 2021];13(4). Disponible sur: https://www.ncbi.nlm.nih.gov/pmc/articles/PMC6488094/
52. Espino A, Gouilly J, Chen Q, Colin P, Guerby P, Izopet J, et al. The mechanisms underlying the immune control of Zika virus infection at the maternal-fetal interface. Front Immunol. 2022;13:1000861.
53. Crooks CM, Weiler AM, Rybarczyk SL, Bliss M, Jaeger AS, Murphy ME, et al. African-lineage Zika virus replication dynamics and maternal-fetal interface infection in pregnant rhesus macaques. J Virol. 2021;95(16):e0222020.
54. Newman CM, Tarantal AF, Martinez ML, Simmons HA, Morgan TK, Zeng X. Early embryonic loss fol-lowing intravaginal Zika virus challenge in rhesus macaques. Front Immunol. 2021;12(1835).
55. Lemos D, Stuart JB, Louie W, Singapuri A, Ramírez AL, Watanabe J, et al. Two sides of a coin: a Zika virus mutation selected in pregnant rhesus macaques promotes fetal infection in mice but at a cost of reduced fitness in nonpregnant macaques and diminished transmissibility by vectors. J Virol. 2020;94(24):e01605-e1620.
56. Alwis de R, Zellweger RM, Chua E, Wang LF, Chawla T, Sessions OM, et al. Systemic inflammation, innate immunity and pathogenesis after Zika virus infection in Cynomolgus Macaques are modulated by strain-specificity within the Asian lineage. Emerg Microbes Infect. 2021;1–31.
57. Hirsch AJ, Smith JL, Haese NN, Broeckel RM, Parkins CJ, Kreklywich C, et al. Zika Virus infection of rhesus macaques leads to viral persistence in multiple tissues. PLOS Pathog. 2017;13(3):e1006219.
58. Lecouturier V, Pavot V, Berry C, Donadieu A, de Montfort A, Boudet F, et al. An optimized purified inactivated Zika vaccine provides sustained immunogenicity and protection in cynomolgus macaques. NPJ Vaccines. 2020;5:19.
59. Nelson BR, Roby JA, Dobyns WB, Rajagopal L, Gale M, Adams Waldorf KM. Immune evasion strategies used by Zika virus to infect the fetal eye and brain. Viral Immunol. 2020;33(1):22–37.
60. Schouest B, Fahlberg M, Scheef EA, Ward MJ, Headrick K, Szeltner DM, et al. Immune outcomes of Zika virus infection in nonhuman primates. Sci Rep. 2020;10:13069.
61. Osuna CE, Lim SY, Deleage C, Griffin BD, Stein D, Schroeder LT, et al. Zika viral dynamics and shedding in rhesus and cynomolgus macaques. Nat Med. 2016;22(12):1448–55.
62. Pantoja P, Pérez-Guzmán EX, Rodríguez IV, White LJ, González O, Serrano C, et al. Zika virus pathogenesis in rhesus macaques is unaffected by pre-existing immunity to dengue virus. Nat Commun. 2017;8(1):15674.
63. Hoen B, Carpentier M, Gaete S, Tressières B, Herrmann-Storck C, Vingadassalom I, et al. Kinetics of anti-Zika virus antibodies after acute infection in pregnant women. J Clin Microbiol. 2019;57(11):e01151-e1219.
64. Haddow AD, Nalca A, Rossi FD, Miller LJ, Wiley MR, Perez-Sautu U, et al. High infection rates for adult macaques after intravaginal or intrarectal inoculation with Zika Virus. Emerg Infect Dis. 2017;23(8):1274–81.

Publisher's Note